

Topological phase transitions and chiral inelastic transport induced by the squeezing of light

Vittorio Peano,¹ Martin Houde,² Christian Brendel,¹ Florian Marquardt,^{1,3} and Aashish A. Clerk²

¹*Institute for Theoretical Physics, University of Erlangen-Nürnberg, Staudtstr. 7, 91058 Erlangen, Germany*

²*Department of Physics, McGill University, 3600 rue University, Montreal, Quebec, H3A 2T8, Canada*

³*Max Planck Institute for the Science of Light, Günther-Scharowsky-Straße 1/Bau 24, 91058 Erlangen, Germany*

(Dated: March 1, 2022)

We show how the squeezing of light can lead to the formation of topological states. Such states are characterized by non-trivial Chern numbers, and exhibit protected edge modes which give rise to chiral elastic and inelastic photon transport. These topological bosonic states are not equivalent to their fermionic (topological superconductor) counterparts and cannot be mapped by a local transformation onto topological states found in particle-conserving models. They thus represent a new type of topological system. We study this physics in detail in the case of a Kagome lattice model, and discuss possible realizations using nonlinear photonic crystals or superconducting circuits.

I. INTRODUCTION

There has been enormous interest in trying to replicate the physics of topological electronic phases in a variety of bosonic systems, including cold atoms [1], photonic systems [2] and more recently phononic systems [3–9]. Photonic analogues include quantum-Hall like states induced through the introduction of synthetic gauge fields [10–16], phases which are analogous to time-reversal invariant topological insulators [17–19], Floquet topological insulators [20, 21] and even Majorana-like modes [22]. Experimental studies of such phases have made significant progress [19, 21, 23–26]. In addition to being of fundamental interest, these topological photonic and phononic phases could have practical utility, as they provide disorder-protected edge modes that could be used for chiral light and sound propagation.

Despite this intense activity, most works on topological bosonic states amount in the end to replicating a well-known fermionic single-particle Hamiltonian with bosons; as the topological properties are a function of the resulting single-particle eigenstates, particle statistics play no crucial role, except perhaps in the methods used for probing the system. As we now discuss, this simple correspondence will fail if the particle number is not conserved.

Consider the most general quadratic Hamiltonian describing bosons on a lattice which respects the discrete translational invariance of the lattice, but which does not conserve particle number:

$$\hat{H} = \sum_{\mathbf{k}, n} \varepsilon_n[\mathbf{k}] b_{\mathbf{k}, n}^\dagger b_{\mathbf{k}, n} + \sum_{\mathbf{k}, n, n'} \left(\lambda_{nn'}[\mathbf{k}] b_{\mathbf{k}, n}^\dagger b_{-\mathbf{k}, n'}^\dagger + h.c. \right) \quad (1)$$

The first term describes a non-interacting band-structure, where \mathbf{k} runs over momenta in the first Brillouin zone, and n labels the bands. The remaining terms correspond to parametric driving or two-mode squeezing terms. As we discuss below, they can be controllably realized in a number of different settings, with the $\hat{b}_{\mathbf{k}, m}$ operators describing "real" particles (i.e. photons in a cavity lattice), and not quasiparticles defined above some

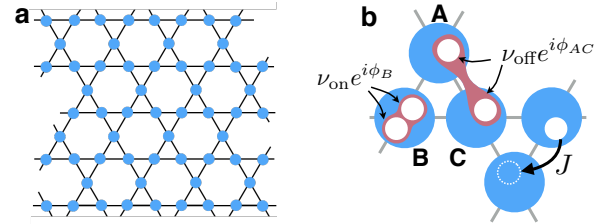


Figure 1. Setup figure: (a) An array of nonlinear cavities forming a kagome lattice. (b) Photons hop between nearest-neighbor sites with rate J . Each cavity is driven parametrically leading to the creation of photon pairs on the same lattice site (rate ν_{on}) and on nearest-neighbor sites (rate ν_{off}). A spatial pattern of the driving phase is imprinted on the parametric interactions, breaking the time-reversal symmetry (but preserving the C_3 rotational symmetry).

effective condensate. While superficially similar to pairing terms in a superconductor, these two-mode squeezing terms have a profoundly different effect in a bosonic system, as there is no limit to the occupancy of a particular single-particle state. They can give rise to highly entangled ground states, and even to instabilities.

Given these differences, it is natural to ask how anomalous "pairing" terms can directly lead to topological bosonic phases. In this work, we study the topological properties of 2D systems described by Eq. (1), in the case where the underlying particle-conserving band structure has no topological structure, and where the parametric driving terms do not make the system unstable. We show that the introduction of particle non-conserving terms can break time-reversal symmetry (TRS) in a manner that is distinct from having introduced a synthetic gauge field, and can lead to the formation of bands having a non-trivial pattern of (suitably defined) quantized Chern numbers. This in turn leads to the formation of protected chiral edge modes: unlike the particle conserving case, these modes can mediate a protected inelastic scattering mechanism along the edge (i.e. a probe field injected into the edge of the sample will travel along the edge, but emerge at a different frequency). In general, the topo-

logical phases we find here are distinct both from those obtained in the particle-conserving case, and from those found in topological superconductors. We also discuss possible realizations of this model using a nonlinear photonic crystal or superconducting microwave circuits.

Note that recent works have explored topological features of bosonic quasiparticles in condensed phases; interactions with the condensate treated at the mean-field level yield a Hamiltonian having the general form of Eq. (1). These include a study of a magnonic crystal [27], as well as general Bose-Einstein condensates in 1D [28] and in 2D [29]. Unlike our work, these studies did not explore the general role that tunable squeezing terms play in yielding topological states. Further, in our case Eq. (1) describes the "real" particles of our system, not quasiparticles defined above some background; this makes detection and potential applications much easier. Most importantly, the topologically-protected inelastic scattering we describe is absent in those different settings.

II. RESULTS

A. Kagome lattice model

For concreteness, we start with a system of bosons on a kagome lattice (see Fig.1),

$$\hat{H}_0 = \sum_{\mathbf{j}} \omega_0 \hat{a}_{\mathbf{j}}^\dagger \hat{a}_{\mathbf{j}} - J \sum_{\langle \mathbf{j}, \mathbf{j}' \rangle} \hat{a}_{\mathbf{j}}^\dagger \hat{a}_{\mathbf{j}'} \quad (2)$$

(we set $\hbar = 1$). Here, we denote by $\hat{a}_{\mathbf{j}}$ the photon annihilation operator associated with lattice site \mathbf{j} , where the vector site index has the form $\mathbf{j} = (j_1, j_2, s)$. $j_1, j_2 \in Z$ labels a particular unit cell of the lattice, while the index $s = A, B, C$ labels the element of the sublattice. $\langle \mathbf{j}, \mathbf{j}' \rangle$ indicates the sum over nearest neighbors, and J is the (real valued) nearest neighbor hopping rate; ω_0 plays the role of an on-site energy. As there are no phases associated with the hopping terms, this Hamiltonian is time-reversal symmetric and topologically trivial. We chose the kagome lattice because it is directly realizable both in quantum optomechanics [5] and in arrays of superconducting cavity arrays [12, 15]; it is also the simplest model where purely local parametric driving can result in a topological phase.

We next introduce quadratic squeezing terms to this Hamiltonian that preserve the translational symmetry of the lattice and that are no more non-local than our original, nearest-neighbor hopping Hamiltonian:

$$\hat{H}_L = -\frac{1}{2} \left[\nu_{\text{on}} \sum_{\mathbf{j}} e^{i\phi_s} \hat{a}_{\mathbf{j}}^\dagger \hat{a}_{\mathbf{j}}^\dagger + \nu_{\text{off}} \sum_{\langle \mathbf{j}, \mathbf{j}' \rangle} e^{i\phi_{s s'}} \hat{a}_{\mathbf{j}}^\dagger \hat{a}_{\mathbf{j}'}^\dagger \right] + h.c. \quad (3)$$

Such terms generically arise from having a nonlinear interaction with a driven auxiliary pump mode on each site (which can be treated classically). As we discuss below, the variation in phases in \hat{H}_L from site to site could

be achieved by a corresponding variation of the driving phase of the pump. Note that we are working in a rotating frame where this interaction is time-independent, and thus ω_0 should be interpreted as the detuning between the parametric driving and the true on-site (cavity) frequency ω_{cav} (i.e. $\omega_0 = \omega_{\text{cav}} - \omega_L/2$, where the parametric driving is at a frequency ω_L). The parametric driving can cause the system to become unstable; we will thus require that the on-site energy ω_0 is always sufficiently large that each parametric driving term is sufficiently non-resonant to ensure stability.

For a generic choice of phases in the parametric driving Hamiltonian of Eq. (3), it is no longer possible to find a gauge where $\hat{H} = \hat{H}_0 + \hat{H}_L$ is purely real when expressed in terms of real-space annihilation operators: hence, even though the hopping Hamiltonian \hat{H}_0 corresponds to strictly zero flux, *the parametric driving can itself break TRS*. In what follows, we will focus for simplicity on situations where time-reversal and particle-conservation are the only symmetries broken by the parametric driving: they will maintain the inversion and C_3 rotational symmetry of the kagome lattice. We will also make a global gauge transformation so that ν_{off} is purely real, while $\nu_{\text{on}} = |\nu_{\text{on}}| e^{i\varphi_\nu}$. In this case, the only possible choices for the ϕ phases have the form $(\phi_A, \phi_B, \phi_C) = (\phi_{AB}, \phi_{BC}, \phi_{CA}) = \pm(0, \delta, 2\delta)$ with $\delta = 2\pi m_\nu/3$, m_ν is an integer and is the vorticity of the parametric pumps.

B. Gap opening and non-trivial topology

\hat{H}_0 is the standard tight-binding kagome Hamiltonian for zero magnetic field, and does not have band gaps: the upper and middle bands touch at the symmetry point $\Gamma \equiv (0, 0)$, whereas the middle and lower bands touch at the symmetry points $K = (2\pi/3, 0)$ and $K' = (\pi/3, \pi/\sqrt{3})$ where they form Dirac cones [see Fig. 2(a)].

Turning on the pairing terms, the Hamiltonian $\hat{H} = \hat{H}_0 + \hat{H}_L$ can be diagonalized in the standard manner as $\hat{H} = \sum_{n, \mathbf{k}} E_n[\mathbf{k}] \hat{\beta}_{n, \mathbf{k}}^\dagger \hat{\beta}_{n, \mathbf{k}}$, where the $\hat{\beta}_{n, \mathbf{k}}$ are canonical bosonic annihilation operators determined by a Bogoliubov transformation of the form (see Appendix A for details):

$$\hat{\beta}_{n, \mathbf{k}}^\dagger = \sum_{s=A, B, C} u_{n, \mathbf{k}}[s] \hat{a}_{\mathbf{k}, s}^\dagger - v_{n, \mathbf{k}}[s] \hat{a}_{-\mathbf{k}, s}. \quad (4)$$

Here, $\hat{a}_{\mathbf{k}, s}$ are the annihilation operators in quasi-momentum space, and $n = 1, 2, 3$ is a band index; we count the bands by increasing energy. The photonic single-particle spectral function now shows resonances at both positive and negative frequencies, $\pm E_n[k]$, corresponding to "particle"- and "hole"-type bands, see Fig. 2(d). Because of the TRS breaking induced by the squeezing terms, the band structure described by $E_n[\mathbf{k}]$ now exhibits gaps, see Fig. 2(b); further, for a finite sized system, one also finds edge modes in the gap, see Fig. 2(d).

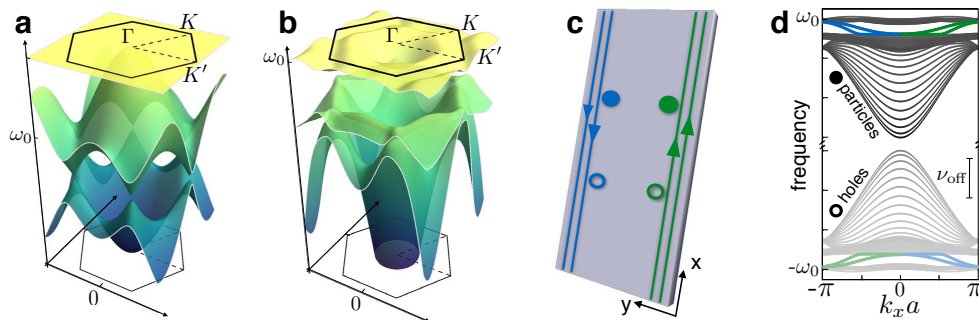


Figure 2. Band structure: (a-b) 3D plots of the bulk band structure for $J = 0.02\omega_0$. The hexagonal Brillouin zone is also shown. (a) In the absence of parametric driving, neighboring bands touch at the rotational symmetry points K and K' and Γ . (b) The parametric driving opens a gap between subsequent bands. For the chosen parameter ($\nu_{\text{on}} = -0.085$ and $\nu_{\text{off}} = 0.22$) there is a global band gap between the second and third band. (d) Hole and particle bands, $\pm E_m[k_x]$, in a strip geometry [sketched in (c)]. The line intensity is proportional to the weight of the corresponding resonance in the photon spectral function, see Appendix E. The edge states localized on the right (left) edge, plotted in green (blue), have positive (negative) velocity.

The above behaviour suggests that the parametric terms have induced a non-trivial topological structure in the wavefunctions of the band eigenstates. To quantify this, we first need to properly identify the Berry phase associated with a bosonic band eigenstate in the presence of particle non-conserving terms. For each \mathbf{k} , the Bloch Hamiltonian $\hat{H}_{\mathbf{k}}$ corresponds to the Hamiltonian of a multi-mode parametric amplifier. Unlike the particle-conserving case, the ground state of such a Hamiltonian is a multi-mode squeezed state with non-zero photon number; it can thus have a non-trivial Berry's phase associated with it when \mathbf{k} is varied, see Appendix B. The Berry phase of interest for us will be the difference of this ground state Berry phase and that associated with a single quasiparticle excitation. One finds that the resulting Berry connection takes the form

$$\mathcal{A}_n = i\langle \mathbf{k}, n | \hat{\sigma}_z \nabla_{\mathbf{k}} | \mathbf{k}, n \rangle, \quad (5)$$

Here, the 6-vector of Bogoliubov coefficients $|\mathbf{k}, n\rangle \equiv (u_{n,\mathbf{k}}[A], u_{n,\mathbf{k}}[B], u_{n,\mathbf{k}}[C], v_{n,\mathbf{k}}[A], v_{n,\mathbf{k}}[B], v_{n,\mathbf{k}}[C])$ plays the role of a single-particle wavefunction, and $\hat{\sigma}_z$ acts in the 'particle-hole-space', associating $+1$ to the u -components and -1 to the v -components, see Appendix B for details. These effective wavefunctions obey the symplectic normalization condition

$$\begin{aligned} \langle \mathbf{k}, n | \hat{\sigma}_z | \mathbf{k}', n' \rangle &= \sum_s u_{n,\mathbf{k}}^*[s] u_{n',\mathbf{k}'}[s] - v_{n,\mathbf{k}}^*[s] v_{n',\mathbf{k}'}[s] \\ &= \delta_{\mathbf{k},\mathbf{k}'} \delta_{n,n'} \end{aligned} \quad (6)$$

Having identified the appropriate Berry connection for a band eigenstate, the Chern number for a band n is then defined in the usual manner:

$$C_n = \frac{1}{2\pi} \int_{BZ} (\nabla \times \mathcal{A}_n) \cdot \hat{z} \quad (7)$$

This definition agrees with that presented in Ref. [27] and (in 1D) Ref. [28]; standard arguments [27] show that

the C_n are integers with the usual properties. We note that, as for superconductors, breaking the $U(1)$ (particle-conservation) symmetry remains compatible with a first-quantized picture after doubling the number of bands. The additional 'hole' bands are connected to the standard 'particle' bands by a particle-hole symmetry; see Appendix A. In bosonic systems, the requirement of stability implies that particle and hole bands can not touch. Thus, the sum of the Chern numbers over the particle bands (with $E > 0$) must be zero, and there cannot be any edge states with energies below the lowest particle bulk band (or in particular, at zero energy); see Appendix B.

In the special case where we only have onsite parametric driving (i.e. $\nu_{\text{off}} = 0, \nu_{\text{on}} \neq 0$), the Chern numbers can be calculated analytically (see Appendix C). They are uniquely fixed by the pump vorticity. If $m_\nu = 0$, we have TRS and the band structure is gapless, while for $m_\nu = \pm 1$, $\vec{C} = (\mp 1, 0, \pm 1)$. This set of topological phases also occurs in a particle-number conserving model on the kagome lattice with a staggered magnetic field, i.e. the Oghushi-Murakami-Nagaosa (OMN) model of the anomalous quantum Hall effect [30, 31].

In the general case, including offsite parametric driving, entirely new phases appear. We have computed the Chern numbers for that case numerically, using the approach of Ref. [32]. In Fig. 3(a), we show the topological phase diagram of our system, where J/ω_0 and m_ν are held fixed, while the parametric drive strengths $\nu_{\text{on}}, \nu_{\text{off}}$ are varied. Different colors correspond to different triplets $\vec{C} \equiv (C_1, C_2, C_3)$ of the band Chern numbers, with gray and dark-gray corresponding to the two phases already present in the OMN model. Strikingly, a finite off-diagonal coupling ν_{off} generates a large variety of phases which are not present in the OMN model. The border between different topological phases represent topological phase transitions, and correspond to parameter values where a pair of bands touch at a particular symmetry point; we discuss this further below.

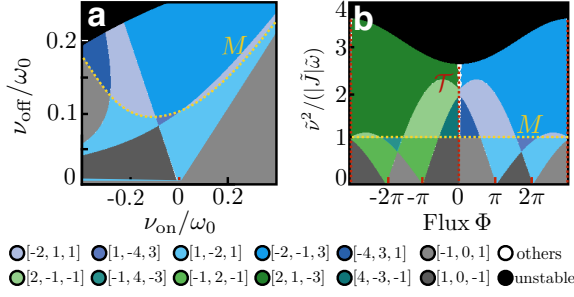


Figure 3. (a) Topological phase diagram for the parametrically driven Kagome lattice model. The y (x) axis corresponds to the strength of the onsite parametric drive ν_{on} (off-site parametric drive ν_{off}), and different colours correspond to different triplets $\vec{C} = (C_1, C_2, C_3)$ of Chern numbers for the three bands of the model. Note that only the gray and dark-gray phases are found in the particle-conserving version of our model with a staggered field. We have fixed the hopping rate $J/\omega_0 = 0.02$, and the vorticity of the pump $m_\nu = 1$. (b) Same phase diagram, but now plotted in terms of the effective flux Φ and effective parametric drive $\tilde{\nu}$ experienced by α quasiparticles. See text for details.

C. Effective model

To gain further insight into the structure of the topological phases found above, it is useful to work in a “dressed-state” basis that eliminates the local parametric driving terms from our Hamiltonian. We thus first diagonalize the purely local terms in the Hamiltonian; for each lattice site \mathbf{j} we have

$$\hat{H}_{\mathbf{j}} = \omega_0 \hat{a}_{\mathbf{j}}^\dagger \hat{a}_{\mathbf{j}} - \frac{1}{2} \left[\nu_{\text{on}} e^{i\phi_{\mathbf{j}}} \hat{a}_{\mathbf{j}}^\dagger \hat{a}_{\mathbf{j}}^\dagger + h.c. \right] = \tilde{\omega} \hat{a}_{\mathbf{j}}^\dagger \hat{a}_{\mathbf{j}}. \quad (8)$$

Here $\tilde{\omega} = \sqrt{\omega_0^2 - \nu_{\text{on}}^2}$, and the annihilation operators $\hat{a}_{\mathbf{j}}$ are given by a local Bogoliubov (squeezing) transformation $\hat{a}_{\mathbf{j}} = e^{i\phi_{\mathbf{j}}} e^{-i\varphi_\nu/2} \left(\cosh r a_{\mathbf{j}} - e^{i\phi_{\mathbf{j}}} e^{i\varphi_\nu} \sinh r \hat{a}_{\mathbf{j}}^\dagger \right)$, where the squeezing factor r is

$$r = \frac{1}{4} \ln \left[\frac{\omega_0 + \nu_{\text{on}}}{\omega_0 - \nu_{\text{on}}} \right]. \quad (9)$$

On a physical level, the local parametric driving terms attempt to drive each site into a squeezed vacuum state with squeeze parameter r ; the $\hat{a}_{\mathbf{j}}$ quasiparticles correspond to excitations above this reference state. Note that we have included an overall phase factor in the definition of the $\hat{a}_{\mathbf{j}}$ which will simplify the final form of the full Hamiltonian.

In this new basis of local quasiparticles, our full Hamiltonian takes the form

$$\hat{H} = \sum_{\mathbf{j}} \tilde{\omega} \hat{a}_{\mathbf{j}}^\dagger \hat{a}_{\mathbf{j}} - \sum_{\langle \mathbf{j}, \mathbf{l} \rangle} \tilde{J}_{\mathbf{j}\mathbf{l}} \hat{a}_{\mathbf{j}}^\dagger \hat{a}_{\mathbf{l}} - \left(\frac{\tilde{\nu}}{2} \sum_{\langle \mathbf{j}, \mathbf{l} \rangle} \hat{a}_{\mathbf{j}}^\dagger \hat{a}_{\mathbf{l}}^\dagger + h.c. \right). \quad (10)$$

The transformation has mixed the hopping terms with the non-local parametric terms: The effective counter-clockwise hopping matrix element is

$$\tilde{J}_{\mathbf{j}\mathbf{l}} = J e^{i\delta} + e^{3i\delta/2} \left[2J \cos \left(\frac{\delta}{2} \right) \sinh^2 r + \nu_{\text{off}} \sinh 2r \cos \left(\frac{\delta}{2} + \varphi_\nu \right) \right], \quad (11)$$

and the magnitude of the effective non-local parametric driving is

$$|\tilde{\nu}| = \left| \nu_{\text{off}} e^{-i(\delta/2 + \varphi_\nu)} + 2\nu_{\text{off}} \cos(\delta/2 + \varphi_\nu) \sinh^2 r + J \sinh 2r \cos(\delta/2) \right|. \quad (12)$$

Note that the phase of $\tilde{\nu}$ can be eliminated by a global gauge transformation, and hence it plays no role; we thus take $\tilde{\nu}$ to be real in what follows.

Our model takes on a much simpler form in the new basis: the onsite parametric driving is gone, and the non-local parametric driving is real. Most crucially, the effective hoppings now can have spatially-varying phases, which depend both on the vorticity of the parametric driving in \hat{H}_L (through δ), and the magnitude of the onsite squeezing (through r). In this transformed basis, the effective hopping phases are the only route to breaking TRS. If the parametric terms were not present, the complex phases would correspond in the usual manner to a synthetic gauge field (i.e. the effective flux Φ piercing a triangular plaquette would be $\Phi = 3 \arg(\tilde{J})$). Our model has thus been mapped on to the standard OMN model for the anomalous quantum Hall effect, with an additional (purely real) nearest-neighbour two-mode squeezing interaction. However, we note that strictly speaking Φ can not be interpreted as a flux in the presence of the additional parametric terms: a ‘flux’ of 2π can not be anymore eliminated by a gauge transformation because the complex phases reappear in the parametric terms. In that case, only a periodicity of 6π in Φ is retained, since that corresponds to having trivial hopping phases of 2π .

Understanding the topological structure of this transformed Hamiltonian is completely sufficient for our purposes: one can easily show that the Chern number of a band is invariant under any local Bogoliubov transformation, hence the Chern numbers obtained from the transformed Hamiltonian in Eq. (8) will coincide exactly with those obtained from the original Hamiltonian in Eq. (3). We thus see that the topological structure of our system is controlled completely through only three dimensionless parameters: the ‘flux’ Φ associated with the hopping phase, the ratio $|\tilde{\nu}/\tilde{J}|$ and the ratio $\tilde{\omega}/|\tilde{J}|$.

The topological phase diagram for the effective model is shown in Fig. 3(b). Again, one sees that as soon as the effective non-local parametric drive $\tilde{\nu}$ is non-zero, topological phases distinct from the standard (particle-conserving) OMN model are possible. The sign of the parametric pump vorticity m_ν determines the sign of the effective flux Φ , c.f. Eq. 11. As such, the right half of

Fig. 3(b) (corresponding to $\Phi > 0$) is a deformed version of the phase diagram of the original model for pump vorticity $m_\nu = 1$, as plotted in Fig. 3(a). Changing the sign of m_ν (and hence Φ) simply flips the sign of all Chern numbers, see Appendix C.

Our effective model provides a more direct means for understanding the boundaries between different topological phases. Most of these are associated with the crossing of bands at one or more high-symmetry points in the Brillouin zone; this allows an analytic calculation of the phase boundary (see Appendix C). Perhaps most striking in Fig. 3(b) is the horizontal boundary (labelled \mathcal{M}), occurring at a finite value of the effective onsite parametric drive, $\tilde{\nu} \approx \sqrt{J\tilde{\omega}}$. This boundary is set by the closing of a band gap at the M points; as these points are associated with the decoupling of one sublattice from the other two, this boundary is insensitive to the flux Φ . Similarly, the vertical line labeled \mathcal{T} denotes a line where the system has TRS, and all bands cross at the symmetry points K , K' and Γ . The case of zero pump vorticity $m_\nu = 0$ (not shown) is also interesting. Here, the effective flux Φ depends on the strength of the parametric drivings, but is always constrained to be 0 or 3π . This implies that the effective Hamiltonian has TRS, even though the original Hamiltonian may not (i.e. if $\text{Im } \nu_{\text{off}} \neq 0$, the original Hamiltonian does not have TRS). For $m_\nu = 0$, the parametric drivings do not open any band gap and the Chern numbers are not well defined.

D. Edge states and transport

Despite their modified definition, the Chern numbers associated with our Bogoliubov bands still guarantee the existence of protected chiral edge modes in a system with boundaries via a standard bulk-boundary correspondence, see Appendix D. These states can be used to transport photons, by exciting them with an auxiliary probe laser beam which is focused on an edge site and at the correct frequency. The lack of particle-number conservation manifests itself directly in the properties of the edge states: along with the standard elastic transmission they can also mediate *inelastic* scattering processes. In terms of the original lab frame, light injected at a frequency ω_p can emerge on the edge at frequency $\omega_L - \omega_p$ where ω_L is the frequency of the laser parametrically driving the system. This is analogous to the idler output of a parametric amplifier. Here, both signal and idler have a topologically protected chirality.

Shown in Fig. 4 are the results of a linear response calculation describing such an experiment, applied to a finite system with corners. We incorporate a finite photon decay rate κ in the standard input-output formalism, see Appendix E for details. Narrow-band probe light inside a topological band gap is applied to a site on the edge, and the resulting inelastic transmission probabilities to each site on the lattice are plotted, see Fig. 4(a). One clearly sees that the probe light is transmitted in a

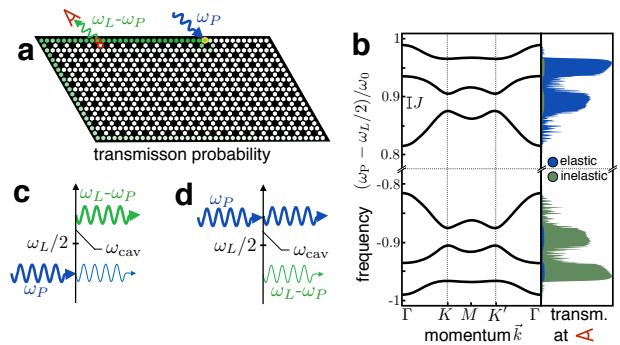


Figure 4. Topologically protected transport in a finite system: (a) A probe beam at frequency ω_p inside the bulk band gap is focused on the edge of a finite sample. The probability map of the light transmitted inelastically at frequency $\omega_L - \omega_p$ clearly shows that the transport is chiral. (b) The elastic and inelastic transmission probability to a pair of sites along the edges [indicated in red in (a)] is plotted in blue and green, respectively. A cut through the bulk bands is shown to the left. (c,d) Sketch of the relevant scattering processes and energy scales. The inelastic (elastic) transmission has a larger rate when the light is injected in the *hole* (*particle*) band gap. Parameters: $J/\omega_0 = 0.02$, $\nu_{\text{on}}/\omega_0 = 0.4$, $\nu_{\text{off}}/\omega_0 = 0.02$, $\kappa/\omega_0 = 0.001$. In (a) $\omega_p - \omega_L/2 = 0.95\omega_0$

uni-directional way along the edge of the sample, and is even able to turn the corner without significant backscatter. The corresponding elastic transmission [not shown] is also chiral and shows the same spatial dependence. In Fig. 4(b) we show the elastic and inelastic transmissions to the sites indicated in red (rescaled by the overall transmission, $1 - R$ where R is the reflection probability at the injection site) as a function of the probe frequency ω_p . By scanning the laser probe frequency one can separately address *particle* and *hole* band gaps. The relative intensity of the inelastic scattering component is highly enhanced when the probe beam is inside a *hole* band gap, see also the sketches in Fig. 4(c-d). When the parametric interaction between the \hat{a} quasiparticles is negligible, the ratio of elastic and inelastic transmissions depends only on the squeezing factor r , [c. f. Eq. (9)], see Appendix E.

E. Physical realization

Systems of this type could be implemented in 2D photonic crystal coupled cavity arrays fabricated from nonlinear optical $\chi^{(2)}$ materials [33–35]. The array of optical modes participating in the transport would be supplemented by pump modes (resonant with the pump laser at twice the frequency). One type of pump mode could be engineered to be spatially co-localized with the transport modes (ν_{on} processes), while others could be located in-between (ν_{off}). The required periodic phase pattern of the pump laser can be implemented using spatial light modulators or a suitable superposition of several laser beams impinging on the plane of the crystal. Optome-

chanical systems offer another route towards generating optical squeezing terms [36, 37], via the mechanically induced Kerr interaction, and this could be exploited to create an optomechanical array with a photon Hamiltonian of the type discussed here. Alternatively, these systems can be driven by two laser beams to create *phononic* squeezing terms [38]. A fourth alternative consists in superconducting microwave circuits of coupled resonators, where Josephson junctions can be embedded to introduce $\chi^{(2)}$ and higher-order nonlinearities, as demonstrated in [39, 40].

III. CONCLUSIONS AND OUTLOOK

In this work, we have shown how tunable squeezing interactions in a photonic system are flexible tools that allow the creation of new kinds of topological bosonic phases. We further demonstrated that the protected edge channels supported by such phases allow uni-directional elastic and inelastic coherent photon transport. Our work opens the door to a number of interesting new directions. On the more practical side, one could attempt to exploit the unique edge states in our system to facilitate directional, quantum-limited amplification. On the more fundamental level, one could use insights from the corresponding disorder problem [41] and attempt to develop a full characterization of particle non-conserving bosonic topological states that are described by quadratic Hamiltonians. This would then be a counterpart to the classification already developed for fermionic systems [42].

VP, CB, and FM acknowledge support by an ERC Starting Grant OPTOMECH, by the DARPA project ORCHID, and by the European Marie-Curie ITN network cQOM. MH and AC acknowledge support from NSERC.

Appendix A: Details of the calculation of the band structure

1. Bogoliubov transformation and first-quantized picture

Here, we show how to find the Bogoliubov transformation Eq. (4) which diagonalizes the Hamiltonian \hat{H} defined in Eqs. (2,3). It is convenient to switch to a first quantized picture by casting the second quantized Hamiltonian \hat{H} in the form

$$\hat{H} = \frac{1}{2} \sum_{\mathbf{k}} \begin{pmatrix} \hat{a}_{\mathbf{k}}^\dagger \\ \hat{a}_{-\mathbf{k}} \end{pmatrix}^T h(\mathbf{k}) \begin{pmatrix} \hat{a}_{\mathbf{k}} \\ \hat{a}_{-\mathbf{k}}^\dagger \end{pmatrix}$$

where $\hat{\mathbf{a}}_{\mathbf{k}} = (\hat{a}_{\mathbf{k}A}, \hat{a}_{\mathbf{k}B}, \hat{a}_{\mathbf{k}C})^T$ and $h(\mathbf{k})$ is the Bogoliubov de Gennes Hamiltonian. By plugging the Bogoliubov ansatz Eq. (4) into the Heisenberg equation of motion

for the normal modes ladder operators $\hat{\beta}_{n,\mathbf{k}}^\dagger$,

$$-i \frac{d}{dt} \hat{\beta}_{n,\mathbf{k}}^\dagger = [\hat{H}, \hat{\beta}_{n,\mathbf{k}}^\dagger] = E_n[\mathbf{k}] \hat{\beta}_{n,\mathbf{k}}^\dagger,$$

one immediately finds the generalized eigenvalue problem

$$\hat{h}(\mathbf{k})|\mathbf{k}_n\rangle = E_n[\mathbf{k}] \hat{\sigma}_z |\mathbf{k}_n\rangle. \quad (\text{A1})$$

Here, the matrix $\hat{\sigma}_z$ is (minus) the identity for the (hole) particle sector,

$$\hat{\sigma}_z = \begin{pmatrix} \mathbb{1}_3 & 0 \\ 0 & -\mathbb{1}_3 \end{pmatrix}.$$

The bosonic quadratic Hamiltonian \hat{H} describes the dynamics linearized around a *stable classical solution* if it is possible to find its normal mode decomposition. In other words, for all \mathbf{k} the eigenvalue problem Eq. (A1) should have a set of three orthonormal (particle-like) solutions, c. f. Eq. (6). A sufficient and necessary criterion for stability is that all eigenvalues of $\hat{\sigma}_z \hat{h}(\mathbf{k})$ are real, see discussion below.

2. Particle-hole symmetry

The symplectic eigenvalue problem (A1) has an embedded particle-hole symmetry: for any particle-like solution with momentum \mathbf{k} , energy $E_n[\mathbf{k}]$, and wavefunction $|\mathbf{k}_n\rangle$ there is a hole-like solution with momentum $-\mathbf{k}$, energy $-E_n[\mathbf{k}]$, and wavefunction

$$|-\mathbf{k}_{-n}\rangle = \sigma_x \mathcal{K} |\mathbf{k}_n\rangle \equiv \mathcal{C} |\mathbf{k}_n\rangle.$$

(notice that the hole-like solutions have negative length $\langle \mathbf{k}_{-n} | \hat{\sigma}_z | \mathbf{k}_{-n} \rangle = -1$). Here, operator \mathcal{K} gives the complex conjugate of the wavefunction and $\hat{\sigma}_x$ exchanges particles and holes,

$$\hat{\sigma}_x = \begin{pmatrix} 0 & \mathbb{1}_3 \\ \mathbb{1}_3 & 0 \end{pmatrix}.$$

In other words, the Bogoliubov de Gennes Hamiltonian has the generalized symmetry $\mathcal{C}^\dagger \hat{h}(\mathbf{k}) \mathcal{C} = -\hat{h}(-\mathbf{k})$ where the charge conjugation operator \mathcal{C} is anti-unitary and $\mathcal{C}^2 = \mathbb{1}_6$. Thus, our system represents the Bosonic analogue of a superconductor in the Class *D* of the standard topological classification.

3. Numerical calculation of the band structure

From Eqs. (2,3) one can immediately derive the explicit expression of the Bogoliubov de Gennes Hamiltonian

$$\hat{h}(\mathbf{k}) = \begin{pmatrix} \omega_0 - J\hat{\tau}(\mathbf{k}) & h_L(\mathbf{k}) \\ h_L^\dagger(\mathbf{k}) & \omega_0 - J\hat{\tau}(\mathbf{k}) \end{pmatrix} \quad (\text{A2})$$

where $\hat{h}_L = -\nu_{\text{on}} \hat{\Lambda}^{m_\nu} - \nu'_{\text{off}} (\hat{\Lambda}^{m_\nu} \hat{\tau} + \hat{\tau} \hat{\Lambda}^{m_\nu})$ (m_ν is the pump vorticity). The matrices $\hat{\tau}(\mathbf{k})$ and $\hat{\Lambda}$ are

single-particle operators acting on the sub-lattice degrees of freedom. They have matrix elements: $\Lambda_{AA} = 1$, $\Lambda_{BB} = e^{i2\pi/3}$, $\Lambda_{CC} = e^{-2i\pi/3}$, $\tau_{BA} = \tau_{AB}^* = 1 + e^{i\mathbf{k}\cdot\mathbf{a}_1}$, $\tau_{CB} = \tau_{BC}^* = 1 + e^{i\mathbf{k}\cdot\mathbf{a}_2}$, $\tau_{AC} = \tau_{CA}^* = 1 + e^{i\mathbf{k}\cdot\mathbf{a}_3}$ where $\mathbf{a}_1 = (-1, -\sqrt{3})$, $\mathbf{a}_2 = (2, 0)$, and $\mathbf{a}_3 = (-1, \sqrt{3})$ are lattice vectors. All other matrix elements are zero. Notice that $\hat{\Lambda}$ raises the quasi-angular momentum by one unit: $\hat{\Lambda}|p, m\rangle = |p, m+1\rangle$ where $|p, m\rangle = (1, \exp[i2m\pi/3], \exp[-i2m\pi/3], 0, 0, 0)$ and likewise for the holes. Here, $m=0$ is the vortex free eigenstate, $m=1$ has a vortex, and $m=-1$ an anti-vortex (m is defined modulo 2). Thus, a hole with quasimomentum m is converted into a particle with quasi-angular momentum $m+m_\nu$. In other words, a pair of down-converted photons have quasi-angular momenta $-m$ and $m_\nu+m$, respectively. The additional quasimomentum m_ν is provided by the pump photons. In order to write the off-diagonal parametric interaction compactly in terms of the quasi-angular momentum raising operator $\hat{\Lambda}$ we have introduced the rescaled off-diagonal parametric coupling $\nu'_{\text{off}} = e^{-i\delta/2}\nu_{\text{off}}$ for pump vorticity $m_\nu = \pm 1$ and $\nu'_{\text{off}} = \nu_{\text{off}}/2$ for pump vorticity $m_\nu = 0$.

For the effective model Eq. (8) the Bogoliubov de Gennes Hamiltonian reads

$$\hat{h}(\mathbf{k}) = \begin{pmatrix} \tilde{\omega} - \tilde{J}\hat{\tau}(\mathbf{k}, \Phi) & -\tilde{\nu}\hat{\tau}(\mathbf{k}) \\ -\tilde{\nu}\hat{\tau}(\mathbf{k}) & \tilde{\omega} - \tilde{J}\hat{\tau}(\mathbf{k}, -\Phi) \end{pmatrix}. \quad (\text{A3})$$

Here, we have introduced the hopping matrix $\hat{\tau}(\mathbf{k}, \Phi)$ in the presence of the synthetic magnetic field flux Φ . It has the following non zero matrix elements: $\tilde{\tau}_{BA} = \tilde{\tau}_{AB}^* = e^{i\Phi/3}(1 + e^{i\mathbf{k}\cdot\mathbf{a}_1})$, $\tilde{\tau}_{CB} = \tilde{\tau}_{BC}^* = e^{i\Phi/3}(1 + e^{i\mathbf{k}\cdot\mathbf{a}_2})$, $\tilde{\tau}_{AC} = \tilde{\tau}_{CA}^* = e^{i\Phi/3}(1 + e^{i\mathbf{k}\cdot\mathbf{a}_3})$. In the most general case, we calculate the band structure and the single-particle wavefunctions by diagonalizing the 6×6 matrix $\hat{\sigma}_z \hat{h}(\mathbf{k})$ numerically.

4. Analytical calculation of the band structure close to the symmetry points

One can gain much insight on the array dynamics, including the stability requirements and the array topology, by calculating analytically the band structure at the symmetry points. This is a particularly easy task at the rotational symmetry points Γ , K , and K' . There, the hopping matrix $\hat{\tau}$ is diagonal in the basis of the quasi-angular momentum eigenstates. Thus, in this basis the Hamiltonian becomes block diagonal with 2-dimensional blocks. Each block is described by a two-mode squeezing Hamiltonian, except for the quasi-momentum $\mathbf{k} = \Gamma$ and $m = -m_\nu$, when it is a single mode squeezing Hamilto-

nian

$$\begin{aligned} \hat{H}_L(\mathbf{k}) &= -\sum_m [\nu_{\text{on}} + \nu'_{\text{off}}(\tau_m + \tau_{m-m_\nu})] \hat{a}_{\mathbf{k},m}^\dagger \hat{a}_{-\mathbf{k},m_\nu-m}^\dagger \\ &\quad + H.c., \quad \text{for } \mathbf{k} = K, K', \\ \hat{H}_L(\Gamma) &= -\left\{ \sum_{m \neq m_\nu} [\nu_{\text{on}} + \nu'_{\text{off}}(\tau_m + \tau_{m-m_\nu})] \hat{a}_{\Gamma,m}^\dagger \hat{a}_{\Gamma,m_\nu-m}^\dagger \right. \\ &\quad \left. - (\nu_{\text{on}}/2 + \nu'_{\text{off}}\tau_{m_\nu}) \hat{a}_{\Gamma,-m_\nu}^{\dagger 2} \right\} + H.c. \end{aligned}$$

where $\hat{a}_{\mathbf{k},m}$ is the creation operator of an excitation with quasimomentum \mathbf{k} ($\mathbf{k} = \Gamma, K, K'$) and quasi-angular momentum m . Moreover, τ_m indicates the corresponding eigenvalue of the hopping matrix $\hat{\tau}$: $\tau_0(\Gamma) = 4$, $\tau_1(\Gamma) = \tau_{-1}(\Gamma) = \tau_1(K) = \tau_{-1}(K') = -2$, $\tau_0(K) = \tau_1(K') = \tau_0(K') = \tau_{-1}(K) = 1$. By diagonalizing the squeezing Hamiltonian we find the general expression for the eigenvalues

$$E_m = -J \frac{\tau_m - \tau_{m-m_\nu}}{2} + \left[\left(\omega_0 - J \frac{\tau_m + \tau_{m-m_\nu}}{2} \right)^2 - |\nu_{\text{on}} + \nu'_{\text{off}}(\tau_m + \tau_{m-m_\nu})|^2 \right]^{1/2}. \quad (\text{A4})$$

From an analogous calculation we obtain the spectrum of the effective model at the rotation symmetry points

$$\tilde{E}_m = \left[\left(\tilde{\omega} - \tilde{J}\tilde{\tau}_m(\Phi) \right)^2 - \tau_m^2 \tilde{\nu}^2 \right]^{1/2} \quad (\text{A5})$$

where $\tilde{\tau}_m(\mathbf{k}, \Phi)$ are the eigenvalues of $\hat{\tau}$: $\tilde{\tau}_0(\Gamma) = 4 \cos[\Phi/3]$, $\tilde{\tau}_{\pm 1}(\Gamma) = 4 \cos[2\pi/3 \mp \Phi/3]$, $\tilde{\tau}_1(K) = \tau_{-1}(K') = -2 \cos[\Phi/3]$, $\tilde{\tau}_1(K') = \tau_0(K) = 2 \cos[\pi/3 - \Phi/3]$, $\tilde{\tau}_{-1}(K) = \tau_0(K') = 2 \cos[\pi/3 + \Phi/3]$.

5. Stability analysis

The system is stable when all eigenvalues of $\hat{\sigma}_z \hat{h}(\mathbf{k})$ are real. If all eigenenergies of the unperturbed Hamiltonian \hat{H}_0 have the same sign the parametric interaction is off-resonant and the system is stable if the parametric couplings are below a finite threshold. On the contrary, if the unperturbed band touches the zero-energy axis, the parametric interaction is resonant for the zero energy modes leading to an instability for any arbitrarily small value of the coupling. Thus, the parametric instability sets an upper limit to the hopping J . For concreteness, we consider a positive onsite energy ω_0 (corresponding to a red detuned drive). In this case, all eigenenergies of \hat{H}_0 are positive if $J < \omega_0/4$. In this case, the system is stable for sufficiently small values of the parametric couplings ν_{on} and ν_{off} . Nevertheless, the threshold of an instability is reached as soon as the lowest eigenenergy of a particle-type band becomes zero for a finite value of the parametric couplings ν_{on} and ν_{off} . For the parameters of Fig. 3 the lowest band touches the zero energy axis at the Γ point. Thus, we can find an analytical expression

for the instability threshold using the solutions at the rotational symmetry points Eqs. (A4,A5). In Fig. 3(a) the state with zero energy at the border of the unstable region has zero quasimomentum and an anti-vortex. Thus, the instability threshold is given by setting $E_{-1}(\Gamma) = 0$. In Fig. 3(b) the state with zero energy has zero quasimomentum and quasi-angular momentum. By setting $\tilde{E}_0(\Gamma) = 0$, we find a simple expression for the instability threshold, $\tilde{\nu} = \tilde{\omega}/4 - \tilde{J} \cos[\Phi/3]$.

Appendix B: Details of the definition and properties of the symplectic Chern number

1. Berry phase of a Bogoliubov quasi-particle

For an excitation conserving Hamiltonian, the Chern number of the m -th band can be viewed as a sum of Berry phases accumulated on a set of closed loops covering the whole Brillouin zone. In this case, the state which accumulates the relevant Berry phase is the m -th eigenstate of the single-particle Hamiltonian $\hat{h}_{\mathbf{k}}$ (a block with quasimomentum \mathbf{k} of the single-particle Hamiltonian \hat{h}). Below, we show that one can naturally extend this definition of the Chern number to any bosonic Hamiltonian including anomalous terms by identifying the relevant Berry phase in a second-quantized setting.

For each quasi-momentum \mathbf{k} , the second-quantized block

$$\hat{H}_{\mathbf{k}} = \begin{pmatrix} \hat{a}_{\mathbf{k}}^\dagger \\ \hat{a}_{-\mathbf{k}} \end{pmatrix}^T h(\mathbf{k}) \begin{pmatrix} \hat{a}_{\mathbf{k}} \\ \hat{a}_{-\mathbf{k}}^\dagger \end{pmatrix}$$

of the full bosonic Hamiltonian \hat{H} is a six-mode squeezing Hamiltonian. If we regard the quasi-momentum \mathbf{k} as an external parameter, we can ask ourselves what is the additional Berry phase accumulated by a single Bogoliubov quasi-particle in a specific band n while the quasi-momentum is varied adiabatically over a closed loop. In other words, we calculate the Berry phase accumulated by the many-body state $\hat{\beta}_{\mathbf{k},n}^\dagger |S_{\mathbf{k}}\rangle$ where $|S_{\mathbf{k}}\rangle$ is the Bogoliubov vacuum. We find

$$\begin{aligned} \varphi_n &= i \oint \langle S_{\mathbf{k}} | \hat{\beta}_{\mathbf{k},n} \nabla_{\mathbf{k}} \hat{\beta}_{\mathbf{k},n}^\dagger | S_{\mathbf{k}} \rangle \cdot d\mathbf{k} \\ &= i \oint \langle S_{\mathbf{k}} | [\hat{\beta}_{\mathbf{k},n}, \nabla_{\mathbf{k}} \hat{\beta}_{\mathbf{k},n}^\dagger] | S_{\mathbf{k}} \rangle \cdot d\mathbf{k} + i \oint \langle S_{\mathbf{k}} | \nabla_{\mathbf{k}} | S_{\mathbf{k}} \rangle \cdot d\mathbf{k} \\ &= i \oint (u_{\mathbf{k},n}^*[s] \nabla_{\mathbf{k}} u_{\mathbf{k},n}[s] - v_{\mathbf{k},n}^*[s] \nabla_{\mathbf{k}} v_{\mathbf{k},n}[s]) \cdot d\mathbf{k} \\ &\quad + i \oint \langle S_{\mathbf{k}} | \nabla_{\mathbf{k}} | S_{\mathbf{k}} \rangle \cdot d\mathbf{k} \\ &= \oint \mathcal{A}_n \cdot d\mathbf{k} + i \oint \langle S_{\mathbf{k}} | \nabla_{\mathbf{k}} | S_{\mathbf{k}} \rangle \cdot d\mathbf{k}. \end{aligned}$$

In the second line we have used that $\hat{\beta}_{\mathbf{k},n} |S_{\mathbf{k}}\rangle = 0$ (by definition of the vacuum). We note that the Bogoliubov vacuum $|S_{\mathbf{k}}\rangle$ is quasi-momentum dependent and

could possibly accumulate a Berry phase by its own, $i \oint \langle S_{\mathbf{k}} | \nabla_{\mathbf{k}} | S_{\mathbf{k}} \rangle \cdot d\mathbf{k} \neq 0$. However, the Berry phase of interest is the additional Berry phase accumulated by the quasi-particle added over the Bogoliubov vacuum.

2. Properties of the symplectic Chern numbers

Taking into account the orthonormality condition Eq. (6), one can immediately prove that the Chern numbers have the usual properties: (i) They are integer numbers; (ii) After a phase transition where two or more bands touch the individual Chern number of the band involved in the crossings may change but their sum does not change. Since the crossing of a particle and hole band lead to an instability rather than a phase transition, the sum of the Chern numbers over the particle bands is zero.

Appendix C: Details of the calculation of the topological phase diagrams

1. Symmetry of the topological phase diagram under synthetic magnetic field inversion

In the topological phase diagram of Fig. 3(b) all Chern numbers change sign if the direction of the synthetic gauge field is inverted, $\Phi \rightarrow -\Phi$. This has a simple explanation: To change the sign of the flux Φ and of the quasimomentum \mathbf{k} corresponds to taking the complex conjugate of the BdG Hamiltonian in momentum space, $\hat{h}(-\mathbf{k}, -\Phi) = \hat{h}^*(\mathbf{k}, \Phi)$, c.f. Eq. A3. It follows that the single-particle eigenfunctions for opposite values of the flux and of the quasi-momentum are also related by complex conjugation, $|\mathbf{k}_n(\Phi)\rangle = (|-\mathbf{k}_n(-\Phi)\rangle)^*$. From the definition of the Chern numbers, c. f. Eq. 7, it immediately follows that the Chern numbers change sign under inversion of the synthetic gauge field Φ .

2. Border of the different topological phases

At a border of a topological phase transition a pair of Chern numbers can change their values because the corresponding bands touch. Generally speaking bands tend to repel each other rather than crossing. However, at a lattice symmetry point this phenomenon does not necessarily occur because the interaction of a pair of bands can be prevented by a selection rule. In particular, at the rotational symmetry points K , K' , and Γ , a hole with quasi-angular momentum m can only be converted into a particle with quasi-angular momentum $m + m_\nu$. We note that due to inversion symmetry the bands must touch simultaneously at the symmetry points K and K' . We refer to the set of parameters where the bands touch at the symmetry points K and K' (Γ) as K -lines (Γ -lines). When also time-reversal symmetry is present there is band crossing at all rotational symmetry

points. We refer to the set of parameters where time-reversal symmetry occurs as \mathcal{T} -lines. In addition, a pair of bands can touch at one of the three M points where one sublattice is decoupled from the remaining two sublattices (a particle or hole on that sublattice can not hop on the remaining sublattices). We note that due to rotational symmetry a pair of bands should touch simultaneously at all three M points. We refer to the set of parameters where a pair of bands touch at the M points as M -lines.

In our highly symmetric system, we expect most of the crossings to occur at a symmetry point. However, we note that accidental crossings away from any symmetry point are not forbidden. Indeed most (but not all) borders of the different topological phases in Fig. 2 can be identified with \mathcal{T} -lines, K -lines, Γ -lines, or M -lines as explained below.

We first focus on the effective model. The vertical lines $\Phi = 0, \pm 3\pi$ are \mathcal{T} -lines (there is time-reversal symmetry because the hopping amplitude \tilde{J} is real). One can also easily recognize the M -lines because they are horizontal. This must be the case because the spectrum at a M -point where a sublattice decouples from the remaining sublattices does not depend on the flux Φ . Indeed, there is such a horizontal line in the phase diagram of Fig. 2(b). We note that it appears for $\tilde{\nu}^2 \approx |\tilde{J}_{ij}| \tilde{\omega}$. Below, we show that this analytical expression holds when the $\hat{\alpha}$ quasi-particles are described by an effective particle-conserving Hamiltonian. We can also find an analytical expression for the K -line and the Γ -lines as explained below.

We initially focus on the Γ -lines. We regard the band crossing condition of a pair of levels with quasi-angular momentum m and m' , $\tilde{E}_m(\Gamma) = \tilde{E}_{m'}(\Gamma)$ as an implicit equation for the parametric coupling $\tilde{\nu}$ as a function of the flux Φ . We take advantage of the analytical expression for the spectrum at the rotational symmetry points Eq. (A5) to solve this equation. For $m = 0$ and $m' = -1$, we find exactly one real positive solution

$$\tilde{\nu} = \frac{1}{2\sqrt{3}} \times \left[\left(\omega_0 - 4\tilde{J} \cos \frac{\Phi}{3} \right)^2 - \left(\omega_0 - 4\tilde{J} \cos \frac{2\pi + \Phi}{3} \right)^2 \right]^{1/2}$$

in the intervals $-3\pi \leq \Phi \leq -\pi$ and $2\pi \leq \Phi \leq 3\pi$. Keeping in mind that the phase diagram is periodic with period 6π , this solution can be thought of as a single Γ -line which goes (for increasing flux) from $\tilde{\nu} = 0$ at $\Phi = 2\pi$ back to $\tilde{\nu} = 0$ at $\Phi = 5\pi$ ($\Phi = -\pi$). Indeed, such a line is visible in the phase diagram of Fig. 2(b). From the implicit equations $\tilde{E}_m(\mathbf{k}) = \tilde{E}_{m'}(\mathbf{k})$, $\mathbf{k} = \Gamma, K$ one can find similar formulas for the remaining Γ -line and the K -lines. In particular, the other Γ -line corresponds to the crossings of the levels with angular-momentum $m = 1$ and $m = 0$ and goes from $\tilde{\nu} = 0$ at $\Phi = \pi$ back to $\tilde{\nu} = 0$ at $\Phi = 4\pi$ ($\Phi = -2\pi$), see also Fig. 2(b). There is not a third Γ -line because the levels with quasi-angular momentum $m = 1$ and $m = -1$ are degenerate only on

the \mathcal{T} -lines. Likewise, one can show that the K -lines go from $\tilde{\nu} = 0$ at $\Phi = -\pi$ back to $\tilde{\nu} = 0$ at $\Phi = \pi$ and from $\tilde{\nu} = 0$ at $\Phi = -2\pi$ back to $\tilde{\nu} = 0$ at $\Phi = 2\pi$, respectively. We note that the formulas for the band crossings are exact and valid for an arbitrary ratio of $\tilde{J}/\tilde{\omega}$. However, if $\tilde{J}/\tilde{\omega}$ is above a finite threshold the unstable region may overlap with the band crossings and not all topological phases will be present in the phase diagram.

Above we have identified all lines forming the border of the different topological phases in Fig. 2(b) except for the lines which appear above the M -lines very close to the \mathcal{T} -lines and surrounds the white areas of the topological phase diagram Fig. 2 b. These lines correspond to accidental crossings which occur away from any symmetry point. They enclose four different topological phases (which are not listed in our legend for brevity).

Next, we discuss the topological phase diagram of the original model. For a pump circulation $m_\nu = 1$ ($m_\nu = -1$), the resulting effective flux Φ is positive (negative), see Eq. (11). Thus, topological phase diagram of the original model is a deformed version of the right (left) half of the effective model phase diagram, see panel (a) of Fig. 2 for the case $m_\nu = 1$ ($m_\nu = -1$). The case $m_\nu = 0$ on the other hand is mapped onto the \mathcal{T} -lines of the effective diagram.

A remarkable feature of our model is that there is only a single topological phase for any fixed value m_ν of the pump circulation if the off-diagonal parametric terms are not present ($\nu_{\text{off}} = 0$): $\vec{C} = (\mp 1, 0, \pm 1)$ for $m_\nu = \pm 1$ and $\vec{C} = (0, 0, 0)$ for $m_\nu = 0$. This is reminiscent of the anomalous Quantum Hall effect on a Kagome lattice with nearest neighbor hoppings (OMN model) where the topological phase is uniquely determined by the sign of the magnetic flux piercing a triangular plaquette, $\vec{C} = (\mp 1, 0, \pm 1)$ if the flux is positive or negative, respectively. Indeed, for small squeezing $\nu_{\text{on}}, J \ll \omega_0$, the parametric interaction effectively induces a small synthetic gauge field with a positive flux for $m_\nu = 1$. This can be easily seen by switching to the effective description and neglecting the residual parametric terms. For concreteness we consider the case $m_\nu = 1$. For small squeezing and $\nu_{\text{off}} = 0$ we are somewhere close to $\tilde{\nu} = 0$, $\Phi = 2\pi$ inside the topological phase $\vec{C} = (-1, 0, 1)$ at the bottom right corner of the effective diagram. From the above analysis of the effective diagram we know that a topological phase transition can occur only if we cross a Γ or \mathcal{T} -line. However, from the analytical solution of the spectrum at the rotational symmetry points of the original model Eq. (A4) we see that such crossings never occur on the $\nu_{\text{off}} = 0$ axis. Thus, there is no topological phase transition even for large squeezing if $\nu_{\text{off}} = 0$.

3. Effective excitation-conserving Hamiltonian

When $\tilde{\omega}$ is much larger than $|\tilde{J}|$ and $\tilde{\nu}$ one can derive an effective excitation conserving Hamiltonian. In the

regime where $\tilde{\nu} \gg |\tilde{J}|$ it is not enough to keep the excitation conserving terms in Eq. (8) but one should also include the leading order correction in $\tilde{\nu}/\tilde{\omega}$. We arrive at the excitation conserving Hamiltonian with next-nearest-neighbor hoppings,

$$\hat{H}_{RW} = \sum_{\mathbf{j}} \tilde{\omega} \hat{\alpha}_{\mathbf{j}}^\dagger \hat{\alpha}_{\mathbf{j}} - \sum_{\langle\langle \mathbf{j}, \mathbf{l} \rangle\rangle} \bar{J}_{\mathbf{j}\mathbf{l}}^{(1)} \hat{\alpha}_{\mathbf{j}}^\dagger \hat{\alpha}_{\mathbf{l}} - \sum_{\langle\langle \mathbf{j}, \mathbf{l} \rangle\rangle} \bar{J}_{\mathbf{j}\mathbf{l}}^{(2)} \hat{\alpha}_{\mathbf{j}}^\dagger \hat{\alpha}_{\mathbf{l}}. \quad (\text{C1})$$

Here, $\langle\langle \mathbf{j}, \mathbf{l} \rangle\rangle$ indicates the sum over next-nearest-neighbor sites and

$$\begin{aligned} \bar{\omega} &= \tilde{\omega} - \frac{2\tilde{\nu}^2}{\tilde{\omega}}, & \bar{J}_{\mathbf{j}\mathbf{l}}^{(2)} &= \frac{\tilde{\nu}^2}{2\tilde{\omega}} \\ \bar{J}_{\mathbf{j}\mathbf{l}}^{(1)} &= \tilde{J}_{\mathbf{j}\mathbf{l}} + \frac{\tilde{\nu}^2}{2\tilde{\omega}}. \end{aligned}$$

In this simplified picture it is straightforward to calculate the band structure at the M points and finding the bad degeneracy condition $\tilde{\nu}^2 = |\tilde{J}_{\mathbf{j}\mathbf{l}}| \tilde{\omega}$ which leads to the horizontal line in the topological phase diagram of the effective model.

Appendix D: Bulk-boundary correspondence

It is well known that in a system with a boundary, the net number of edge states (the number of right-movers minus the number of left-movers) in a bulk band gap is a topological invariant [43]. This statement is based on the sole assumption that the band structure and the corresponding eigenvectors change smoothly in the presence of a local perturbation that does not close a gap. Thus, it clearly applies to any quadratic Hamiltonian. For the special case of an excitation-conserving insulator or a superconductor the bulk boundary correspondence expresses such topological invariant in terms of the Chern numbers: the net number of edge states in a band gap coincides with the sum of the Chern numbers of all bands below that band gap. Here, we explicitly show that the bulk-boundary correspondence is still valid for our model where anomalous terms are present.

We start noticing that the wavefunctions of the RWA Hamiltonian Eq. (C1) depend only on two parameters: the phase $\Phi/3$ of \tilde{J} and the dimensionless next-nearest-neighbor coupling $\tilde{\nu}^2/(|\tilde{J}|\tilde{\omega})$. By calculating the phase diagram as a function of these parameters [not shown] we see that it supports all topological phases present in the topological phase diagram of the effective Hamiltonian for the $\hat{\alpha}$ -quasiparticles [our full model without approximations]. Thus, we can continuously interpolate between the two Hamiltonians without crossing any topological phase transition [by sending $\tilde{\omega} \rightarrow \infty$ while also tuning Φ and $\tilde{\nu}^2/(|\tilde{J}|\tilde{\omega})$ to stay in the same topological phase]. Keeping in mind that the bulk-boundary correspondence holds for the excitation-conserving Hamiltonian Eq. (C1) and that the net number of edge states does not change during the interpolation [unless a gap is closed], we can

conclude that such correspondence is valid for our model even for small $\tilde{\omega}$ where the RWA leading to Eq. (C1) is not a good approximation.

We note that the above reasoning combined with the assumption that a continuous interpolation between any quadratic bosonic Hamiltonian and an excitation conserving Hamiltonian is always possible without closing any band gap, leads to the general validity of the bulk-edge correspondence.

Appendix E: Details of the transport calculations

In our transport calculations we have included photon decay. We adopt the standard description of the dissipative dynamics of photonic systems in terms of the Langevin equation of input-output theory [44], for each site:

$$\dot{\hat{a}}_j = i\hbar^{-1}[\hat{H}, \hat{a}_j] - \kappa \hat{a}_j/2 + \sqrt{\kappa} \hat{a}_j^{(\text{in})}. \quad (\text{E1})$$

In practice, we consider an array of detuned parametric amplifiers with intensity decay rate κ and add to the standard description of each parametric amplifier the inter-cell coherent coupling described in the main text. The last term describes the input field and includes the vacuum fluctuations as well as the influence of an additional probe field. The field leaking out of each cavity at site j is given by the input-output relations $\hat{a}_j^{(\text{out})} = \hat{a}_j^{(\text{in})} - \sqrt{\kappa} \hat{a}_j$. The above formulas give an accurate description of a photonic system where the intrinsic losses during injection and inside the system are negligible.

In Fig. (3), we show the probabilities $T_E(\omega, l, j)$ and $T_I(\omega, l, j)$ that a photon injected on site j with frequency $\omega_{\text{in}} = \omega + \omega_L/2$ is transmitted to site l elastically (at frequency $\omega + \omega_L/2$) or inelastically (at frequency $\omega_L/2 - \omega$) where it is detected. From the Kubo formula and the input-output relations we find

$$\begin{aligned} T_E(\omega, l, j) &= |\delta_{lj} - i\kappa \tilde{G}_E(\omega, l, j)|^2 \\ T_I(\omega, l, j) &= \kappa^2 |\tilde{G}_I(\omega, l, j)|^2. \end{aligned}$$

They depend on the Green's function in frequency space $\tilde{G}(\omega, l, j) = \int_{-\infty}^{\infty} dt e^{i\omega t} G(t, l, j)$ where

$$G(t, i, j) = \begin{pmatrix} G_E(t, l, j) & G_I^*(t, l, j) \\ G_I(t, l, j) & G_E^*(t, l, j) \end{pmatrix}$$

with the elastic and inelastic components $G_E(t, l, j) = -i\Theta(t)\langle[\hat{a}_l(t), \hat{a}_j^\dagger(0)]\rangle$ and $G_I(t, l, j) = -i\Theta(t)\langle[\hat{a}_j^\dagger(t), \hat{a}_l^\dagger(0)]\rangle$, respectively. From the Kubo formula and the input-output relations $\hat{a}_j^{(\text{out})} = \hat{a}_j^{(\text{in})} - \sqrt{\kappa} \hat{a}_j$ we find

$$T_E(\omega, l, j) = |\delta_{lj} - i\kappa \tilde{G}_E(\omega, l, j)|^2 \quad (\text{E2})$$

$$T_I(\omega, l, j) = \kappa^2 |\tilde{G}_I(\omega, l, j)|^2. \quad (\text{E3})$$

Taking into account that

$$\hat{a}_j(t) = \sum_n e^{-iE[n]t} u_n[j] \hat{b}_n + e^{iE[n]t} v_n^*[j] \hat{b}_n^\dagger$$

where \hat{b}_n are the ladder operators of the normal modes for a finite array of N sites and $|n\rangle = (u_n[1], \dots, u_n[N], v_n[1], \dots, v_n[N])^T$ are the corresponding *single-particle* states, the Green's function reads

$$G_E(\omega, l, j) = \sum_n \frac{u_n[l]u_n^*[j]}{\omega - E[n] + i\kappa/2} - \frac{v_n^*[l]v_n[j]}{\omega + E[n] + i\kappa/2}, \quad (\text{E4})$$

$$G_I(\omega, l, j) = \sum_n \frac{v_n[l]u_n^*[j]}{\omega - E[n] + i\kappa/2} - \frac{u_n^*[l]v_n[j]}{\omega + E[n] + i\kappa/2}. \quad (\text{E5})$$

We note that for a probe field inside the bandwidth of the particle (hole) sector but far detuned from the hole (particle) sector, only the first (second) term of the summand in Eq. (E4) and (E5) is resonant. Thus, as expected, the inelastic scattering is comparatively larger when the probe field is in the hole band gap.

It is easy to estimate quantitatively the relative in-

tensities of elastically and inelastically transmitted light when the parametric interaction of the $\hat{\alpha}$ quasiparticles is small. In this case, it is straightforward to show that $|v_n[j]/u_n[j]| \approx \tanh r$ independent of the band n and the site j . By putting together Eqs. (E2,E3,E4,E5) and neglecting the off-resonant terms we find that for $\omega, \tilde{\omega} \gg |\tilde{J}|, \kappa, |\omega - \tilde{\omega}|$,

$$\begin{aligned} T_I(\omega, l, j) &\approx (\tanh r)^2 T_E(\omega, l, j) \\ &\approx T_I(-\omega, l, j) \approx (\coth r)^2 T_E(-\omega, l, j). \end{aligned}$$

These analytical formulas agree quantitatively with the numerical results shown in Fig. 4(b) [note that in Fig. 4(b) the transmission at the output sites is rescaled by the overall transmission, $\sum_{l \neq j} T_I(\omega, l, j) + T_E(\omega, l, j)$].

Note that we have assumed, for simplicity, that there is no intrinsic absorption present. If there is intrinsic photon absorption, that will add another decay channel to the equation for the light field, but the resulting picture for the light field propagation remains unchanged except for the expected reduction in propagation length along the edge state.

-
- [1] N. Goldman, G. Juzeliūnas, P. Öhberg, and I. B. Spielman, Reports on Progress in Physics **77**, 126401 (2014).
- [2] L. Lu, J. D. Joannopoulos, and M. Soljacic, Nat Photon **8**, 821 (2014), ISSN 1749-4885.
- [3] E. Prodan and C. Prodan, Phys. Rev. Lett. **103**, 248101 (2009).
- [4] C. L. Kane and T. C. Lubensky, Nat. Phys. **10**, 39 (2013), 1308.0554.
- [5] V. Peano, C. Brendel, M. Schmidt, and F. Marquardt, Phys. Rev. X **5**, 031011 (2015).
- [6] Z. Yang, F. Gao, X. Shi, X. Lin, Z. Gao, Y. Chong, and B. Zhang, Phys. Rev. Lett. **114**, 114301 (2015).
- [7] R. Süsstrunk and S. D. Huber, Science **349**, 47 (2015).
- [8] J. Paulose, B. G.-g. Chen, and V. Vitelli, Nat. Phys. **11**, 153 (2015).
- [9] L. M. Nash, D. Kleckner, A. Read, V. Vitelli, A. M. Turner, and W. T. M. Irvine, arXiv:1504.03362v2 (2015).
- [10] F. D. M. Haldane and S. Raghu, Phys. Rev. Lett. **100**, 013904 (2008).
- [11] S. Raghu and F. D. M. Haldane, Phys. Rev. A **78**, 033834 (2008).
- [12] J. Koch, A. A. Houck, K. L. Hur, and S. M. Girvin, Phys. Rev. A **82**, 043811 (2010).
- [13] R. O. Umucalilar and I. Carusotto, Phys. Rev. A **84**, 043804 (2011).
- [14] K. Fang, Z. Yu, and S. Fan, Nature Photonics **6**, 782 (2012).
- [15] A. Petrescu, A. A. Houck, and K. Le Hur, Phys. Rev. A **86**, 053804 (2012).
- [16] M. Schmidt, S. Kessler, V. Peano, O. Painter, and F. Marquardt, Optica **2**, 635 (2015).
- [17] M. Hafezi, E. A. Demler, M. D. Lukin, and J. M. Taylor, Nat. Phys. **7**, 907 (2011).
- [18] A. B. Khanikaev, S. H. Mousavi, W.-K. Tse, M. Kargarian, A. H. MacDonald, and G. Shvets, Nature Materials **12**, 233 (2012).
- [19] M. Hafezi, S. Mittal, J. Fan, A. Migdall, and J. M. Taylor, Nature Photonics **7**, 1001 (2013).
- [20] T. Kitagawa, M. A. Broome, A. Fedrizzi, M. S. Rudner, E. Berg, I. Kassal, A. Aspuru-Guzik, E. Demler, and A. G. White, Nat Commun **3**, 882 (2012).
- [21] M. C. Rechtsman, Y. Plotnik, J. M. Zeuner, D. Song, Z. Chen, A. Szameit, and M. Segev, Phys. Rev. Lett. **111**, 103901 (2013).
- [22] C.-E. Bardyn and A. İmamoğlu, Phys. Rev. Lett. **109**, 253606 (2012).
- [23] Z. Wang, Y. Chong, J. D. Joannopoulos, and M. Soljacic, Nature **461**, 772 (2009).
- [24] M. C. Rechtsman, J. M. Zeuner, Y. Plotnik, Y. Lumer, D. Podolsky, F. Dreisow, S. Nolte, M. Segev, and A. Szameit, Nature **496**, 196 (2013).
- [25] S. Mittal, J. Fan, S. Faez, A. Migdall, J. M. Taylor, and M. Hafezi, Phys. Rev. Lett. **113**, 087403 (2014).
- [26] L. D. Tzuang, K. Fang, P. Nussenzveig, S. Fan, and M. Lipson, Nature Photonics **8**, 701 (2014).
- [27] R. Shindou, R. Matsumoto, S. Murakami, and J.-i. Ohe, Phys. Rev. B **87**, 174427 (2013).
- [28] G. Engelhardt and T. Brandes, arXiv:1503.02503v1 (2015).
- [29] C.-E. Bardyn, T. Karzig, G. Refael, and T. C. H. Liew, arXiv:1503.08824v1 (2015).
- [30] K. Ohgushi, S. Murakami, and N. Nagaosa, Phys. Rev. B **62**, R6065 (2000).
- [31] D. Green, L. Santos, and C. Chamon, Phys. Rev. B **82**, 075104 (2010).
- [32] T. Fukui, Y. Hatsugai, and H. Suzuki, Journal of the Physical Society of Japan **74**, 1674 (2005).
- [33] S. Mookherjea and A. Yariv, Ieee J Quantum Elect **8**, 448 (2002).
- [34] B. J. Eggleton, B. Luther-Davies, and K. Richardson, Nat Photonics **5**, 141 (2011).
- [35] J. Dahdah, M. Pilar-Bernal, N. Courjal, G. Ulliac, and

- F. Baida, *J. Appl. Phys.* **110**, (2011).
- [36] A. H. Safavi-Naeini, S. Gröblacher, J. T. Hill, J. Chan, M. Aspelmeyer, and O. Painter, *Nature* **500**, 185 (2013).
- [37] T. P. Purdy, P. L. Yu, R. W. Peterson, N. S. Kampel, and C. A. Regal, *Phys. Rev. X* **3**, 031012 (2013).
- [38] A. Kronwald, F. Marquardt, and A. A. Clerk, *Phys. Rev. A* **88**, 063833 (2013).
- [39] N. Bergeal, R. Vijay, V. E. Manucharyan, I. Siddiqi, R. J. Schoelkopf, S. M. Girvin, and M. Devoret, *Nat. Phys.* **6**, 296 (2010).
- [40] B. Abdo, A. Kamal, and M. Devoret, *Phys. Rev. B* **87**, 014508 (2013).
- [41] V. Gurarie and J. T. Chalker, *Phys. Rev. B* **68**, 134207 (2003).
- [42] S. Ryu, A. P. Schnyder, A. Furusaki, and A. W. W. Ludwig, *New J. Phys.* **12**, 065010 (2010).
- [43] M. Z. Hasan and C. L. Kane, *Rev. Mod. Phys.* **82**, 3045 (2010).
- [44] A. A. Clerk, M. H. Devoret, S. M. Girvin, F. Marquardt, and R. J. Schoelkopf, *Reviews of Modern Physics* **82**, 1155 (2010), 0810.4729.